UCRL-18535

cy. 2

University of California

Ernest O. Lawrence Radiation Laboratory

RECEIVED
LAWRENCE
RADIATION LABORATORY

DEC 16 1968

LIBRARY AND
DOCUMENTS SECTION

ELECTRON AND BREMSSTRAHLUNG-INDUCED FISSION OF HEAVY AND MEDIUM-HEAVY NUCLEI

L. G. Moretto, R. C. Gatti, S. G. Thompson, J. T. Routti,
J. H. Heisenberg, L. M. Middleman, M. R. Yearian and R. Hofstadter

October 18, 1968

TWO-WEEK LOAN COPY

This is a Library Circulating Copy which may be borrowed for two weeks. For a personal retention copy, call Tech. Info. Division, Ext. 5545

UCRL-18535 cy. 2

DISCLAIMER

This document was prepared as an account of work sponsored by the United States Government. While this document is believed to contain correct information, neither the United States Government nor any agency thereof, nor the Regents of the University of California, nor any of their employees, makes any warranty, express or implied, or assumes any legal responsibility for the accuracy, completeness, or usefulness of any information, apparatus, product, or process disclosed, or represents that its use would not infringe privately owned rights. Reference herein to any specific commercial product, process, or service by its trade name, trademark, manufacturer, or otherwise, does not necessarily constitute or imply its endorsement, recommendation, or favoring by the United States Government or any agency thereof, or the Regents of the University of California. The views and opinions of authors expressed herein do not necessarily state or reflect those of the United States Government or any agency thereof or the Regents of the University of California.

Submitted to Physical Review

UCRL-18535
Preprint

UNIVERSITY OF CALIFORNIA

Lawrence Radiation Laboratory
Berkeley, California

AEC Contract No. W-7405-eng-48

ELECTRON AND BREMSSTRAHLUNG-INDUCED FISSION OF HEAVY AND MEDIUM-HEAVY NUCLEI

L. G. Moretto, R. C. Gatti, S. G. Thompson, J. T. Routti,
J. H. Heisenberg, L. M. Middleman, M. R. Yearian and R. Hofstadter

October 18, 1968

photoproduction at energies near 140 MeV. The π meson produced inside the nucleus was thought to be reabsorbed producing high excitation energy. Since this paper was published the same effect was observed in other isotopes and was always attributed to the onset of π meson photoproduction.[5,8,9] Attempts were not usually made to consider separately the behavior of the fission probability as distinct from the interaction cross section, nor to take into account the energy deposition associated with each interaction process.

In the present work these effects are taken into account separately and it is found that the variation in the photofission cross section as a function of energy for elements in the region of bismuth or lighter is essentially accounted for by the increase in fission probability with increasing excitation energy. On the other hand, since the fission probability in uranium is practically constant as a function of energy, the energy dependence of its photofission cross section is a reflection of the interaction cross section. It seems also that the interaction described by the quasi-deuteron model[10] is on the average much more efficient in transferring energy to the nucleus than is the mechanism involving π meson photoproduction. Consequently the former interaction process appears to be the dominant one in the excitations of sufficient energy to cause fission of lighter nuclei where the fission barriers are of large magnitude. On the other hand both processes are important in the fission of heavier nuclei, such as uranium, which have small fission barriers.

In the present work we have measured the electron and Bremsstrahlung induced fission cross sections of the nuclei $^{238}_{92}U$, $^{209}_{83}Bi$, $^{208}_{82}Pb$, $^{174}_{70}Yb$, and $^{154}_{62}Sm$ over the energy range 60 to 1000 MeV. By applying the theoreti-

cal expressions for the energy distribution of the virtual photon spectrum associated with electrons, we have calculated the photofission cross sections from the electron-induced fission cross section data. Then the photofission cross sections calculated above have been integrated over the Bremsstrahlung spectrum and found to be in agreement with the measured Bremsstrahlung induced fission cross sections. This procedure has been followed assuming the virtual photon spectra corresponding to E1, M1, and E2 transitions, and some information about multipolarity has been obtained. The photofission cross sections have been subsequently analyzed in terms of the contributions due to photon interaction and to the fission probability. The nature of the energy dependence of the photofission cross section has been established.

II. THEORETICAL RELATIONS

A. Bremsstrahlung-Induced Reaction Cross Sections

The Bremsstrahlung-induced reaction cross sections are related to the photon-induced reaction cross sections through the following expression

$$\sigma_B = \int_0^{E_o} \sigma_\gamma(E)\, K^B(E_o,E)\, dE \quad , \tag{1}$$

where σ_B is the Bremsstrahlung induced reaction cross section, $\sigma_\gamma(E)$ is the photo reaction cross section and $K^B(E_o,E)$ is the energy distribution of the Bremsstrahlung from a thin radiator. This last quantity is given by the following relation[11]

$$K^B(E_o,E) = \frac{1}{E}\frac{X}{\ln(183Z^{-1/3})}\left\{\left[1 + \left(1 - \frac{E}{E_o + m}\right)^2 - \frac{2}{3}\left(1 - \frac{E}{E_o + m}\right)\right] \times \ln(183Z^{-1/3}) + \frac{1}{9}\left(1 - \frac{E}{E_o + m}\right)\right\} , \quad (2)$$

where E_o is the electron energy, E is the photon energy, m is the rest energy of the electron, Z is the atomic number of the radiator and X is the thickness of the radiator expressed in radiation lengths. The above relation assumes complete screening which applies when the electron energy is high.

B. Electron-Induced Reaction Cross Sections

Within the Weizsacker-Williams approximation,[1] the electromagnetic interaction between nuclei and electrons can be expressed in terms of a virtual photon spectrum associated with an electron of energy E_o available for producing nuclear excitations of energy E and multipolarity ℓ. This allows one to relate the electron-induced reaction cross section to the photo-reaction cross section as follows:

$$\sigma_e = \int_0^{E_o} \sigma_\gamma(E)\, K^e(E_o,E,\ell)\, dE \quad , \quad (3)$$

where σ_e is the electron-induced reaction cross section and $K^e(E_o,E,\ell)$ is the energy distribution of the virtual photon spectrum associated with the electron. The theoretical expressions for $K^e(E_o,E,\ell)$ on the assumption of a point nucleus are[12]

$$K^e(E_o,E,\ell) = \frac{\alpha}{\pi}\frac{1}{E}\left\{\left[1+\left(\frac{E_o - E}{E_o}\right)^2\right]\ln\left(\frac{2E_o(E_o - E)}{m\,E}\right) - C_\ell\right\} \quad , \tag{4}$$

where E is the energy of the virtual photon, α is the fine structure constant, m is the electron rest energy and

$$C_\ell = \begin{cases} 2\,\dfrac{(E_o - E)}{E_o} & \text{for E1 transitions} \\ 0 & \text{for M1 transitions} \\ -8/3\left(\dfrac{E_o - E}{E}\right)^2 & \text{for E2 transitions} \end{cases} \quad .$$

It appears that the simultaneous measurement of the Bremsstrahlung and electron-induced reaction cross sections allows one to check the validity and consistency of the quantities $K^B(E_o,E)$ and $K^e(E_o,E,\ell)$ and could even give some indication as regards the multipolarity of the interaction.

III. EXPERIMENTAL

A. Electron Beam

The beam of electrons in the energy range between 60 and 1000 MeV was provided by the Stanford Mark III Electron Linear Accelerator. The beam was deflected twice before entering the target area which is separated by heavy shielding from the rest of the accelerator; with these precautions the beam has been found to be essentially free of Bremsstrahlung photons.[13]

A quadrupole focussing lens was used to focus the beam on the thin targets within an area of diameter 5 mm. The reading of the beam was

performed with a Faraday cup. The total number of electrons striking the target was obtained by integrating the electron-beam current. A schematic drawing of the experimental arrangement is given in Fig. 1.

B. Target Assembly and Fission Fragment Detectors

The targets were obtained by evaporating the metals of the nuclei $^{154}_{62}Sm$, $^{170}_{70}Yb$, $^{208}_{82}Pb$, $^{209}_{83}Bi$ and $^{238}_{92}U$ as the fluoride on aluminum foils of thickness 1.8 mg/cm^2. The thickness of the targets was chosen such that the effect of the Bremsstrahlung generated in them would be insignificant with respect to the overall fission rate induced by electrons. Weights of the various targets were as follows: $^{238}_{92}U$ = 0.0856 mg/cm^2 and 0.0145 mg/cm^2; $^{209}_{83}Bi$ = 1.060 mg/cm^2 and 1.214 mg/cm^2; $^{208}_{82}Pb$ = 1.901 mg/cm^2 and 2.160 mg/cm^2; $^{170}_{70}Yb$ = 0.300 mg/cm^2 and $^{154}_{62}Sm$ = 0.200 mg/cm^2. The targets were located in the center of small fission chambers, facing the beam at angles of 45°, as shown in Fig. 1.

Strips of mica held against the cylindrical walls of the chambers were used to detect the fission fragments. The configuration of the assembly allowed the measurement of the fission fragment angular distribution over angles ranging from 45° to 205° with respect to the beam direction.

Fission chambers of two sizes were used: the larger version (63.5 mm radius) was used when an accurate angular distribution was required or when the fission cross section was sufficiently large, and the smaller version (28.4 mm radius) was used to obtain total fission cross sections only. All the fission chambers could be provided with aluminum radiators of different thickness in front of the targets.

Several fission chambers were usually stacked on a ladder contained in a large vacuum chamber. The ladder could be moved vertically by remote control in such a way as to move the various targets sequentially into the beam position without breaking the vacuum. The fission fragments were prevented from entering the wrong chamber by aluminum shielding of 0.1 mm thickness.

After the bombardments the exposed mica strips were etched for approximately four hours in 48% hydrofluoric acid, and the fission tracks were observed[14] with an optical microscope under 100× magnification and counted. The scanning was performed continuously from 90° to $\sim 170^{\circ}$ whenever the angular distribution was to be checked or the smallness of the cross section was such as to require improved statistics. Otherwise the scanning was performed at $\sim 90^{\circ}$ over an area sufficient to give $\sim 3\%$ statistical accuracy.

C. Data Collection

In order to observe electron induced fission the data were collected in the energy region from 60 to 1000 MeV for all the targets without using any radiator. Then an aluminum radiator of thickness 0.0173 radiation lengths was used in order to observe Bremsstrahlung-induced fission. The thickness of the radiator was chosen such as to approximately double the fission rate induced by the pure electron beam.

With such data it is possible to determine the ratio between electron and Bremsstrahlung-induced fission. However, to gather more accurate information, the relative cross sections for three different radiator thicknesses were measured for all the targets at an energy of 650 MeV.

IV. EXPERIMENTAL RESULTS

A. Angular Distribution

The fission fragment angular distributions for both Bremsstrahlung and electron-induced fission are expected to be isotropic in the energy range covered by the experiments. In fact, the small angular momentum orientation brought in by the photon is more than offset by the effect of the fast cascade and by the particle evaporation. The expectation has been checked by our experiment which showed no anisotropy within the error limits.

B. Cross Sections

The experimental cross sections for electron-induced fission are presented in Table 1 and Fig. 2. In Table 2 and Fig. 3 the effective cross sections for fission induced by electrons plus Bremsstrahlung produced by 0.0173 rad. lengths of aluminum are presented; in Fig. 4 the Bremsstrahlung-induced fission cross sections per equivalent quantum are presented. Figure 5 also presents the effective fission cross sections as a function of the radiator thicknesses at 650 MeV electron energy.

C. Errors

The statistical errors associated with the measurements are usually of the order of 3%. However, another source of random errors was introduced by the changes in solid angle associated with small displacements in the location of electron beam from the center of the target. Although no special effort has been made to estimate the magnitude of such an effect, the data are consistent with an overall error not smaller than 5% and not much larger than 10%.

Two ^{238}U targets were used: one of thickness 0.0856 mg/cm^2 and the other 0.0145 mg/cm^2, the first determined by alpha particle spectrometry and the second by gross alpha counting. In the latter case the uncertainty in the measurement was of the order of 20%. Comparison of the two sets of cross section data showed a systematic difference of ~ 20%. Therefore the cross sections obtained from bombardments of the thinner target were normalized on the basis of cross sections obtained from the thicker target. In all the other cases where two targets were used for the same isotope, the target thicknesses were taken at face value as determined by weighing and normalization was not performed.

It can be seen from Figs. 3 and 4 that, aside from the uranium case, the cross sections of all the other target nuclei decrease steeply with decreasing energy. However, the cross sections for the Yb and Sm isotopes show a flattening at the lowest electron energies at a value of approximately 10^{-33} cm^2. This effect is most likely due to contamination of the targets with about one part per million of thorium or uranium. These impurities would account for the effect and therefore the lowest energy points were corrected in the analysis of the results and the interpretation.

V. DISCUSSION

A. Consistency of the Electron and Bremsstrahlung Kernels—Photofission Cross Sections

The photofission cross sections were obtained by unfolding the electron induced fission cross sections using the expressions (4) to represent the virtual photon spectra. This operation was performed by using an iterative method developed for the numerical solution of the first order Fredholm integral equation.[15] The procedure employed combines the information contained in the measured data with physical a priori information about the solution such as nonnegativity and non-oscillatory behavior. Within these constraints a well defined solution is obtained without making any prescription regarding its shape.

The integral equation is approximated by a matrix equation using piecewise linear representations for both the kernel and the solution vector; thus the solution may assume any general form. A quadratic form is defined which is composed of the weighted square deviations between the measured data points and the calculated responses and the norm of the numerical logarithmic second difference of the solution, the latter term being used to prevent unwanted oscillations. The quadratic form is minimized with respect to the parameters defining the solution in non-negative subspace. The method allows determination of many more points in the solution vector than there are in the measured spectrum. This assures adequate resolution and a good match to the experimental data. The computations were performed using a CDC-6600 computer.

The unfolding was also performed with the three kernels corresponding to E1, M1, and E2 transitions. The unfolded curves were integrated back into the same kernels in order to check how accurately the experimental data are fitted. The photofission cross sections, together with the experimental electron-induced fission cross sections and the fits to them corresponding to the solutions of the unfolding procedure are shown in Figs. 6 to 10 for the case of the E1 kernel. The E1 and M1 kernels generate very similar unfolded curves, which, when folded back, fit the data with the same good accuracy. On the other hand the E2 kernels generate unfolded curves that, when folded back, do not fit the data quite satisfactorily as shown for the one example ($^{238}_{92}U$) in Fig. 11. In this case it is impossible to obtain a closer fit to the data within the physical constraints inherent in the unfolding procedure as described above. For the lighter nuclei the fits obtained using the E2 kernels were also consistently worse than the ones obtained with E1 or M1 kernels but were not as unsatisfactory as the example shown in Fig. 11 for $^{238}_{92}U$.

This seems to rule out any substantial contribution of E2 transitions in the excitation of $^{238}_{92}U$ and to suggest predominant excitation through E1 or M1 transitions for the other isotopes. The similarity between the solutions obtained with the E1 and M1 kernels is such that it seems impossible to decide in favor of either one.

To check the consistency of the electron and Bremsstrahlung kernels, each of the solutions from the unfolding procedure was also folded back into the Bremsstrahlung kernel (2) corresponding to an aluminum radiator of thickness 0.0173 radiation lengths. To these calculated Bremsstrahlung-

induced fission cross sections, the contributions from the experimentally determined electron induced fission cross sections were added. Now one can compare these results with the same quantities determined directly from the experiments as given in Fig. 3 and Table 1. The comparison is shown in Fig. 12. Here again the E1 kernel was used. The agreement is satisfactory, showing that it is possible to transform the electron-induced fission cross sections to the Bremsstrahlung-induced fission cross sections and vice versa. Again equally satisfactory results can be obtained with the M1 kernel. As far as the E2 kernel is concerned, the unfolding produces solutions which are not quite consistent with the experimental data as seen above and which are also highly non-unique. Therefore, the operation of folding the solutions obtained with the E2 kernel into the Bremsstrahlung spectrum is unreliable and does not provide any information.

The agreement between electron and Bremsstrahlung data can also be seen in Fig. 5. Here the experimental effective fission cross sections as a function of radiator thickness are presented. The data were taken at 650 MeV electron energy. The solid line was calculated again by unfolding the electron fission cross section and folding it back into the Bremsstrahlung distribution. The agreement appears to be satisfactory.

B. Energy Dependence of Photofission Cross Sections

It will be shown here that the increase of the photo fission cross section as a function of energy for the lighter nuclei is due primarily to the energy dependence of the fission probability.

The ratio of the fission width over the neutron width $\frac{\Gamma_f}{\Gamma_n}$ can be calculated from statistical considerations[16] as

$$\frac{\Gamma_f}{\Gamma_n} = K_o \frac{a_n}{a_f} \frac{\left[2a_f^{\frac{1}{2}} (E_x - B_f)^{\frac{1}{2}} - 1\right]}{4A^{2/3} (E_x - B_n)} \exp \left[2a_f^{\frac{1}{2}} (E_x - B_f)^{\frac{1}{2}} - 2a_n^{\frac{1}{2}} (E_x - B_n)^{\frac{1}{2}}\right] , \tag{5}$$

where E_x is the excitation energy, B_f is the fission barrier, B_n is the neutron binding energy, a_f and a_n are the level density parameters at the fission saddle point and for the residual nucleus after neutron evaporation respectively, K_o is a numerical constant and A is the mass number of the nucleus. For $E_x \gg B_f$ and $E_x \gg B_n$ and $a_f = a_n = a$ we obtain the following high energy limit:

$$\ln \frac{\Gamma_f}{\Gamma_n} = \ln \left(\frac{K_o a^{\frac{1}{2}} (E_x - B_f)^{\frac{1}{2}}}{2A^{2/3} (E_x - B_n)} \right) - a^{\frac{1}{2}} (B_f - B_n) E^{-\frac{1}{2}} . \tag{6}$$

For high Z nuclei, as in our case, the charged particle evaporation is small with respect to neutron emission because of the influence of the Coulomb barrier and thus $\Gamma_{tot} \simeq \Gamma_f + \Gamma_n$. For $\frac{\Gamma_f}{\Gamma_n} \ll 1$ we have also $\frac{\Gamma_f}{\Gamma_{tot}} \simeq \frac{\Gamma_f}{\Gamma_n}$.

The fission cross section for any reaction can be written as: $\sigma_f = \sigma_o P_f$, where σ_o is the effective cross section for the compound nucleus formation and P_f is the total fission probability. The total fission probability P_f should not be identified with the quantity $\frac{\Gamma_f}{\Gamma_{tot}}$ because the former includes not only the so-called "first chance" fission, but also the fissions occurring after the emission of the nth neutron. However, it is expected that the fission probability P_f retains the same energy dependence as $\frac{\Gamma_f}{\Gamma_{tot}}$. We write then:

$$\ln \sigma_f = \ln \sigma_o - E_x^{-\frac{1}{2}} \bar{a}^{\frac{1}{2}} (\bar{B}_f - \bar{B}_n) + C \quad . \tag{7}$$

Here $\bar{a}$, $\bar{B}_f$, $\bar{B}_n$ are expected to be some kind of averages of the respective quantities a, B_f, B_n for the nuclei along the evaporation chain and C is a quantity varying very slowly with the energy.

Before making use of the above relation, we test it with ^{4}He induced fission cross section data where the quantity σ_o is well understood and evaluated by an optical model calculation. In Fig. 13 the quantity $\frac{\sigma_f}{\sigma_o}$ is plotted as a function of $E_x^{-\frac{1}{2}}$ on a semilog scale for the reactions ^{206}Pb(^{4}He,fission),[17] ^{197}Au(^{4}He,fission)[17] and ^{184}W(^{4}He,fission).[18] It is seen that the predicted linear dependence is nicely reproduced.

We can now plot in the same way the photofission cross sections of ^{209}Bi, ^{208}Pb, ^{174}Yb and ^{154}Sm obtained by the unfolding of the respective electron-induced fission cross sections. We observe a remarkable linearity of the plot from the lowest energies up to approximately 250 MeV as shown in Figs. 14, 15, 16 and 17. It is to be noticed that in this

interval the cross sections span three or four orders of magnitude. This behavior is very similar to that of the ^{4}He induced fission for the isotopes mentioned above. It is reasonable then to conclude that the energy dependence of the photofission cross section is simply due to the energy dependence of the fission probability. This proof can be carried one step further. If it is true that the main increase in the photofission cross section is due to the energy dependence of the fission probability, it must also be true that the total photon absorption cross section must remain essentially constant in the energy range where the plot of the photofission cross section is linear with $E^{-\frac{1}{2}}$.

To estimate the total photon absorption cross section we use the expression proposed by Levinger[10] on the basis of the quasi deuteron model which is

$$\sigma_o \simeq 8 \frac{NZ}{A} \sigma_D \quad , \tag{8}$$

where σ_D is the deuteron photo-disintegration cross section[19] as given in Fig. 18 and N, Z and A are the neutron, proton and mass number of the isotope in question. We see that the fast decrease of the cross section with increasing energy is interrupted by the isobar resonance, which makes the cross section approximately constant over the energy range where we expected it to be constant from the analysis of the photofission cross sections (80 - 250 MeV).

Using for σ_o the expression (8) we can calculate the absolute value of the quantity $\sigma_f/\sigma_o = P_f$ for all the isotopes (Figs. 14, 15, 16 and 17). We observe that the elimination of the σ_o energy dependence both improves

and extends the linearity of the plot over the energy range up to 400 MeV and over four orders of magnitude. The slopes of the curves are observed to become steeper the lighter the Z of the nucleus is. This is consistent with the expectation that the fission barriers increase with decreasing Z^2/A. Even the absolute value of $P_f = \sigma_f/\sigma_o$ seems very plausible as compared with the P_f in ^{4}He induced fission of ^{206}Pb, ^{197}Au and ^{184}W. A further confirmation of the goodness of the absolute value of σ_f/σ_o in ^{209}Bi and ^{208}Pb comes from the data reported by Goldanski et al.[20] They have measured the fission cross section of ^{208}Pb and ^{209}Bi bombarded with 120 MeV neutrons. The quantities σ_f/σ_o obtained from such data are shown for comparison with our data in Figs. 16 and 17 and are seen to be in very good agreement with our results.

The conclusion at this point seems to be that the energy dependence of the photofission cross section is well understood if we take into account the proper energy dependence of the fission probability and we use the interaction cross section predicted by the quasi deuteron model. However there is still an unexplained discrepancy in the case of ^{238}U. For this isotope the fission probability is very close to one at all excitation energies. It would then be expected that the ^{238}U photofission cross section should reflect the interaction cross section predicted by the quasi deuteron model. Examination of Fig. 10 shows that this is true only up to an energy of 200 MeV. Above this energy the cross section increases as much as four times the expected value on the basis of the quasi deuteron model. Therefore, some other mechanism seems to play a significant role above 200 MeV. The work of Roos and Peterson[22] indicates that π meson photoproduction comes substantially into play at about this energy on the basis of their measurements of the production of stars in nuclear emulsion,

as shown in Fig. 19. It is especially significant to observe that their cross section curve agrees quantitatively with our photofission cross section curve for ^{238}U shown in Fig. 10. Then if it is true that this mechanism has an influence in the case of ^{238}U, the question arises as to why it is not also contributing to the photofission cross section of the other isotopes.

We suggest that the explanation may reside in the following two factors: (1) The amount of excitation energy resulting from the two types of interactions that may be considerably different; (2) The large difference in the magnitude of the fission barriers of uranium as compared with the lighter elements. Large differences in fission probability are known to result from moderate changes in the magnitudes of fission barriers.

The quasi deuteron absorption mechanism seems to be very efficient in producing highly excited nuclei; in this mechanism the absorbed photon transfers its energy to a neutron-proton pair. As far as the energy deposition is concerned, a 200 MeV photon interacting by this mechanism will have the same probability of transferring a given amount of energy as a 100 MeV proton and 100 MeV neutron.

On the other hand if the absorption of the photon occurs via π meson photo-production, the π meson has to be reabsorbed by interacting with a pair of nucleons in order to have the same chance of transferring the same energy as in the quasi deuteron interaction.

The mean free path of a π meson in a heavy nucleus varies with its kinetic energy; it is very large at low energies, it is still 1.0 nuclear radius at 100 MeV and it reaches a minimum of $\sim$ 0.1 nuclear radius at 200 MeV.[22] In the photon energy range studied, the π mesons, when pro-

duced, have rather small kinetic energy and therefore good probability of escaping from the nucleus.

In the cases where the π meson escapes directly from the nucleus or is elastically scattered one or more times before leaving the nucleus, the energy deposition is substantially smaller than that associated with the quasi deuteron interaction. Here the fission barrier comes into play. For a nucleus with a low fission barrier such as ^{238}U ($\sim$ 6 MeV), all of the above described processes will make the nucleus undergo fission with probability close to one whenever the energy deposited is larger than 6 MeV. For a nucleus with a high fission barrier (20 - 40 MeV) such as bismuth and lighter isotopes an energy much larger than the fission barrier is required in order to give a substantial fission probability. Therefore, all the processes in which the π meson escapes will be relatively ineffective in inducing fission while these processes would give rise to the stars observed in nuclear emulsions. This explains why the quasi deuteron mechanism above seems to be required in order to explain the behavior of photofission cross sections of bismuth and lighter elements.

It is interesting to notice that the large photofission cross section in ^{238}U at low energy shown in Fig. 10 which is due mainly to the giant resonance absorbtion together with the approximate $\frac{1}{E}$ dependence of the Bremsstrahlung or virtual photon spectrum explains the predominance of low energy excitations which are well known to give asymmetric fission in the heaviest elements. Such asymmetric fission has been observed in ^{238}U bombarded with electrons of energy 250 MeV[13] and with Bremsstrahlung of 1500 and 3000 MeV.[23]

ACKNOWLEDGMENTS

We are grateful for the valuable assistance of G. Garabedian, M. Lombardo, G. Towns and K. Miles in scanning the mica strips. We are especially indebted to Joan Phillips for assistance with the preparation and typing of this paper. We wish to acknowledge valuable suggestions concerning the theoretical aspects of this paper by J. D. Walecka.

FOOTNOTES AND REFERENCES

* Work done under the auspices of the U. S. Atomic Energy Commission and the U. S. Office of Naval Research Contract [Nonr 225(67)].

† On leave from Laboratorio di Radiochimica, Università di Pavia, Pavia, Italy.

‡ Work supported in part by the "Bundesministerium für Wissenschaft und Forschung," Germany.

1. K. F. Weizsacker, Z. Physik 88, 612 (1934); E. J. Williams, Phys. Rev. 45, 729 (1934).
2. G. Bernardini, R. Reitz and E. Segrè, Phys. Rev. 90, 573 (1953).
3. R. A. Schmitt and N. Sugarman, Phys. Rev. 95, 1260 (1954).
4. L. Katz, T. M. Kavanagh, A. G. W. Cameron, E. C. Bailery and J. W. T. Spinks, Phys. Rev. 99, 98 (1955).
5. J. A. Jungerman and H. M. Steiner, Phys. Rev. 106, 585 (1957).
6. E. V. Minarek and V. A. Novikov, Soviet Phys.—JETP 5, 253 (1957).
7. H. G. de Carvalho, A. Celano, G. Cortini, G. Chigo and R. Rinzivillo, Nuovo Cimento 19, 187 (1961); H. G. de Carvalho, G. Cortini, E. Del Giudice, G. Potenza and R. Rinzivillo, Nuovo Cimento 32, 293 (1964).
8. Yu. N. Ranyuk and P. V. Sorokin, Yad. Fiz. 5, 531 (1967) [Sov. Nucl. Phys. 5, 377 (1967)].
9. A. V. Mitrofanova, Yu. N. Ranyuk and P. V. Sorokin, Yad. Fiz. 6, 703 (1967) [Sov. Nucl. Phys. 6, 512 (1968)].
10. J. S. Levinger, Nuclear Photo-Disintegration, Oxford University Press, London, 1960.

11. Bruno Rossi, High Energy Particles, Prentice Hall, Englewood Cliffs, New Jersey, 1956, p. 48.

12. W. C. Barber, Phys. Rev. 111, 1642 (1958).

13. H. R. Bowman, R. C. Gatti, R. C. Jared, G. Kilian, L. G. Moretto, S. G. Thompson, M. R. Croissiaux, J. H. Heisenberg, R. Hofstadter, L. M. Middleman and M. R. Yearian, Phys. Rev. 168, 1396 (1968).

14. P. B. Price and R. M. Walker, J. Appl. Phys. 33, 2625 (1962); J. Appl. Phys. 33, 3407 (1962).

15. J. T. Routti, Lawrence Radiation Laboratory Report UCRL-18514, in preparation.

16. J. R. Huizenga, R. Chaudhry and R. Vandenbosch, Phys. Rev. 126, 210 (1962).

17. S. G. Thompson, Arkiv Fysik 36, 267 (1967).

18. L. G. Moretto, R. C. Gatti and S. G. Thompson, Lawrence Radiation Laboratory Report UCRL-17989, Nuclear Chemistry Division Annual Report, p. 141.

19. J. S. Levinger, Phys. Rev. 97, 970 (1955).

20. V. I. Goldanski, V. S. Penkina and E. A. Tamurov, Soviet Phys.—JETP 29, 778 (1955); Soviet Phys.—JETP 2, 677 (1956).

21. Charles E. Roos and Vincent Z. Peterson, Phys. Rev. 124, 1610 (1961).

22. Earl K. Hyde, The Nuclear Properties of the Heavy Elements, Prentice Hall, Englewood Cliffs, New Jersey, 1964, Vol. III, p. 435; N. Metropolis, R. Bivius, M. Storm, J. M. Miller, G. Friedlander and Anthony Turkevich, Phys. Rev. 110, 204 (1958); S. J. Lindenbaum and Luke C. L. Yuan, Phys. Rev. 100, 306 (1955).

23. I. R. Williams, C. B. Gulmer, G. F. Dell, M. J. Engebretson, Phys. Letters 26B, 140 (1968).

Table 1. Electron induced fission cross sections (cm^2).

Energy (MeV)	$^{238}_{92}U$	$^{209}_{83}Bi$	$^{208}_{82}Pb$	$^{174}_{70}Yb$		$^{154}_{62}Sm$	
60	$(4.32\pm0.16)\times10^{-27}$	$(7.06\pm0.47)\times10^{-32}$	$(6.86\pm0.84)\times10^{-33}$	$(5.39\pm1.12)\times10^{-33}$	----- [a]		
100	$(4.79\pm0.13)\times10^{-27}$	$(6.66\pm0.58)\times10^{-31}$	$(2.41\pm0.10)\times10^{-31}$	$(4.73\pm1.67)\times10^{-33}$	----- [a]	$(3.07\pm1.53)\times10^{-33}$	----- [b]
150	$(5.59\pm0.20)\times10^{-27}$	$(5.24\pm0.16)\times10^{-30}$	$(1.25\pm0.04)\times10^{-30}$	$(1.10\pm0.08)\times10^{-32}$	$(4.60\pm0.08)\times10^{-33}$ [a]	$(3.70\pm0.45)\times10^{-33}$	$(5.0\pm4.5)\times10^{-34}$ [b]
200	$(6.08\pm0.19)\times10^{-27}$	$(1.05\pm0.04)\times10^{-29}$	$(3.04\pm0.09)\times10^{-30}$	$(2.52\pm0.19)\times10^{-32}$	$(1.79\pm0.19)\times10^{-32}$ [a]	$(3.79\pm0.70)\times10^{-33}$	$(2.9\pm7.0)\times10^{-34}$ [b]
250	$(5.95\pm0.22)\times10^{-27}$	$(2.26\pm0.10)\times10^{-29}$	$(7.82\pm0.21)\times10^{-30}$	$(7.03\pm0.43)\times10^{-32}$	$(6.24\pm0.43)\times10^{-32}$ [a]	$(1.04\pm0.16)\times10^{-32}$	$(6.5\pm1.6)\times10^{-33}$ [b]
300	$(6.84\pm0.19)\times10^{-27}$		$(1.48\pm0.05)\times10^{-29}$	$(2.28\pm0.07)\times10^{-31}$	$(2.20\pm0.07)\times10^{-31}$ [a]		
350	$(7.62\pm0.25)\times10^{-27}$	$(5.36\pm0.23)\times10^{-29}$	$(2.85\pm0.06)\times10^{-29}$	$(6.34\pm0.25)\times10^{-31}$	$(6.25\pm0.25)\times10^{-31}$ [a]	$(4.62\pm0.22)\times10^{-32}$	$(4.18\pm0.22)\times10^{-32}$ [b]
450	$(8.37\pm0.24)\times10^{-27}$	$(7.63\pm0.29)\times10^{-29}$	$(3.99\pm0.13)\times10^{-29}$	$(1.44\pm0.05)\times10^{-30}$	$(1.43\pm0.05)\times10^{-30}$ [a]	$(9.62\pm0.69)\times10^{-32}$	$(9.12\pm0.69)\times10^{-32}$ [b]
500	$(9.51\pm0.33)\times10^{-27}$	$(8.74\pm0.28)\times10^{-29}$					
550	$(1.00\pm0.03)\times10^{-26}$	$(1.18\pm0.04)\times10^{-28}$	$(6.26\pm0.19)\times10^{-29}$	$(2.52\pm0.08)\times10^{-30}$	$(2.51\pm0.08)\times10^{-30}$ [a]	$(1.93\pm0.08)\times10^{-31}$	$(1.88\pm0.08)\times10^{-31}$ [b]
583	$(1.07\pm0.03)\times10^{-26}$	$(1.13\pm0.04)\times10^{-28}$					
600			$(6.63\pm0.21)\times10^{-29}$	$(3.57\pm0.12)\times10^{-30}$	$(3.56\pm0.12)\times10^{-30}$ [a]		
650	$(9.98\pm0.33)\times10^{-27}$	$(1.38\pm0.04)\times10^{-28}$	$(7.25\pm0.23)\times10^{-29}$	$(4.41\pm0.19)\times10^{-30}$	$(4.40\pm0.04)\times10^{-30}$ [a]	$(2.40\pm0.13)\times10^{-31}$	$(2.34\pm0.13)\times10^{-31}$ [b]
750	$(1.03\pm0.03)\times10^{-26}$	$(1.49\pm0.04)\times10^{-28}$	$(8.99\pm0.30)\times10^{-29}$	$(5.90\pm0.47)\times10^{-30}$	$(5.89\pm0.47)\times10^{-30}$ [a]		
800						$(5.13\pm0.21)\times10^{-31}$	$(5.07\pm0.21)\times10^{-31}$ [b]
900	$(1.14\pm0.04)\times10^{-26}$	$(1.72\pm0.05)\times10^{-28}$	$(1.17\pm0.04)\times10^{-28}$	$(7.43\pm0.23)\times10^{-30}$	$(7.42\pm0.23)\times10^{-30}$ [a]		
1000	$(1.09\pm0.03)\times10^{-26}$	$(1.90\pm0.08)\times10^{-28}$	$(1.30\pm0.04)\times10^{-28}$	$(9.53\pm0.31)\times10^{-30}$	$(9.52\pm0.31)\times10^{-30}$ [a]	$(8.96\pm0.30)\times10^{-31}$	$(8.90\pm0.30)\times10^{-31}$ [b]

[a] Corrected for one part per million of ^{238}U impurity.

[b] Corrected for five parts per ten million of ^{238}U impurity.

Table 2. Electron plus Bremsstrahlung induced fission cross sections (cm^2). The Bremsstrahlung radiation is produced by the electron beam striking 0.0173 radiation lengths of aluminum radiator.

Energy (MeV)	$^{238}_{92}U$	$^{209}_{83}Bi$	$^{208}_{82}Pb$	$^{174}_{70}Yb$	$^{154}_{62}Sm$
60	$(5.34 \pm 0.19) \times 10^{-27}$	$(6.21 \pm 0.98) \times 10^{-32}$	$(7.99 \pm 0.31) \times 10^{-33}$	$(9.56 \pm 1.60) \times 10^{-33}$	
100	$(8.62 \pm 0.24) \times 10^{-27}$	$(1.13 \pm 0.03) \times 10^{-30}$	$(3.58 \pm 0.16) \times 10^{-31}$	$(6.41 \pm 1.31) \times 10^{-33}$	
150	$(8.96 \pm 0.27) \times 10^{-27}$	$(7.68 \pm 0.33) \times 10^{-30}$	$(1.48 \pm 0.06) \times 10^{-30}$	$(1.38 \pm 0.29) \times 10^{-32}$	
200	$(1.12 \pm 0.03) \times 10^{-26}$	$(1.70 \pm 0.06) \times 10^{-29}$	$(6.94 \pm 0.23) \times 10^{-30}$	$(7.79 \pm 0.45) \times 10^{-32}$	$(9.15 \pm 0.92) \times 10^{-33}$
250	$(9.37 \pm 0.28) \times 10^{-27}$	$(3.62 \pm 0.12) \times 10^{-29}$		$(1.97 \pm 0.14) \times 10^{-31}$	$(1.84 \pm 0.22) \times 10^{-32}$
300	$(1.25 \pm 0.04) \times 10^{-26}$	$(7.46 \pm 0.24) \times 10^{-29}$	$(3.54 \pm 0.12) \times 10^{-29}$	$(6.68 \pm 0.24) \times 10^{-31}$	
350	$(1.52 \pm 0.05) \times 10^{-26}$	$(8.91 \pm 0.29) \times 10^{-29}$	$(4.79 \pm 0.17) \times 10^{-29}$	$(1.50 \pm 0.04) \times 10^{-30}$	$(8.69 \pm 0.35) \times 10^{-32}$
400	$(1.41 \pm 0.04) \times 10^{-26}$	$(1.47 \pm 0.05) \times 10^{-28}$	$(7.54 \pm 0.19) \times 10^{-29}$	$(2.10 \pm 0.07) \times 10^{-30}$	
450	$(1.49 \pm 0.05) \times 10^{-26}$	$(1.72 \pm 0.06) \times 10^{-28}$	$(9.37 \pm 0.32) \times 10^{-29}$	$(3.42 \pm 0.11) \times 10^{-30}$	$(1.94 \pm 0.10) \times 10^{-31}$
500	$(1.53 \pm 0.04) \times 10^{-26}$	$(1.96 \pm 0.07) \times 10^{-28}$			
550	$(1.64 \pm 0.06) \times 10^{-26}$	$(1.95 \pm 0.06) \times 10^{-28}$	$(1.11 \pm 0.03) \times 10^{-28}$	$(4.70 \pm 0.14) \times 10^{-30}$	$(4.63 \pm 0.17) \times 10^{-31}$
583	$(1.82 \pm 0.06) \times 10^{-26}$	$(2.16 \pm 0.06) \times 10^{-28}$			
600			$(1.29 \pm 0.05) \times 10^{-28}$	$(6.07 \pm 0.19) \times 10^{-30}$	
650	$(1.60 \pm 0.05) \times 10^{-26}$	$(2.45 \pm 0.06) \times 10^{-28}$	$(1.47 \pm 0.05) \times 10^{-28}$	$(8.53 \pm 0.33) \times 10^{-30}$	$(5.52 \pm 0.26) \times 10^{-31}$
750	$(1.77 \pm 0.06) \times 10^{-26}$	$(3.22 \pm 0.12) \times 10^{-28}$	$(1.92 \pm 0.06) \times 10^{-28}$	$(9.10 \pm 0.03) \times 10^{-30}$	
800					$(1.14 \pm 0.04) \times 10^{-30}$
900	$(1.91 \pm 0.04) \times 10^{-26}$	$(2.91 \pm 0.10) \times 10^{-28}$	$(1.88 \pm 0.06) \times 10^{-28}$	$(1.37 \pm 0.03) \times 10^{-29}$	$(9.13 \pm 0.45) \times 10^{-31}$
1000	$(1.73 \pm 0.05) \times 10^{-26}$	$(3.14 \pm 0.10) \times 10^{-28}$	$(1.86 \pm 0.06) \times 10^{-28}$	$(1.36 \pm 0.04) \times 10^{-29}$	$(1.66 \pm 0.06) \times 10^{-30}$

Fig. 14. Photofission cross section (triangles, left scale) and fission probability σ_f/σ_o (solid circles, right scale) as a function of $E_x^{-\frac{1}{2}}$ for $^{209}_{83}Bi$. The point indicated by a square is the fission probability calculated from the data of Goldanski et al.[20]

Fig. 15. Photofission cross section (triangles, left scale) and fission probability σ_f/σ_o (solid circles, right scale) as a function of $E_x^{-\frac{1}{2}}$ for $^{208}_{82}Pb$. The point indicated by a square is the fission probability calculated from the data of Goldanski et al.[20]

Fig. 16. Photofission cross section (triangles, left scale) and fission probability σ_f/σ_o (solid circles, right scale) as a function of $E_x^{-\frac{1}{2}}$ for $^{174}_{70}Yb$.

Fig. 17. Photofission cross section (triangles, left scale) and fission probability σ_f/σ_o (solid circles, right scale) as a function of $E_x^{-\frac{1}{2}}$ for $^{154}_{62}Sm$.

Fig. 18. The total cross section for the deuteron photo effect plotted against photon energy W on a log-log scale from Levinger.[19]

Fig. 19. Summation of the cross sections for high energy photo-processes as a function of photon energy from Roos and Peterson.[22]

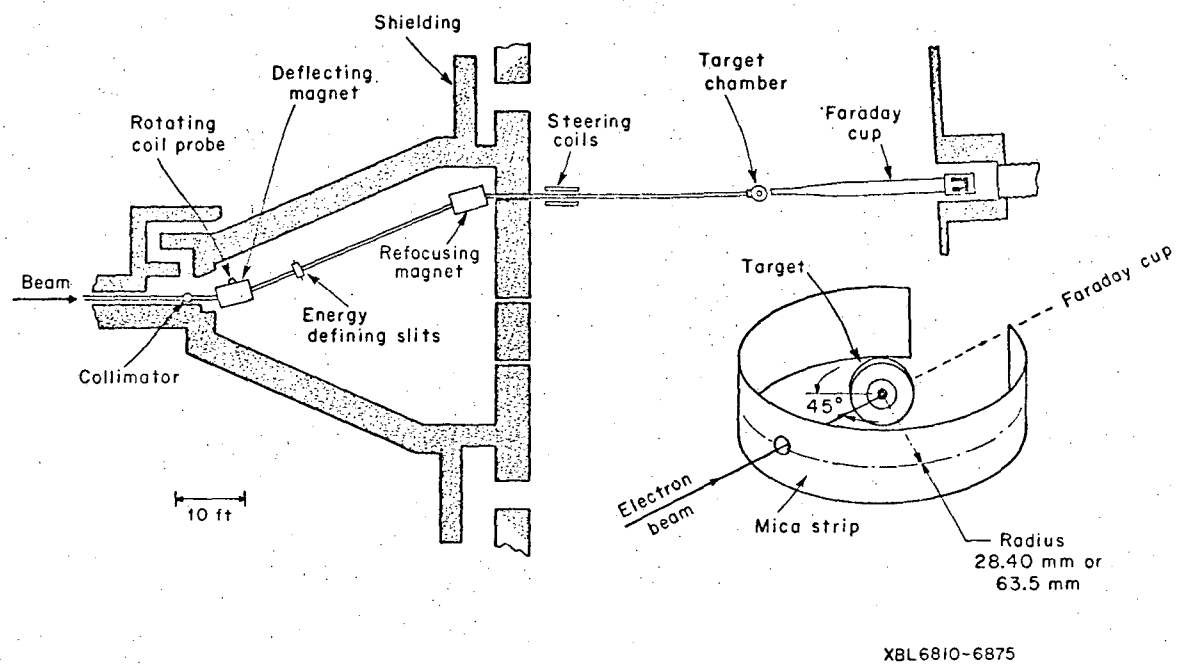
Shielding
Deflecting magnet
Rotating coil probe
Steering coils
Target chamber
Faraday cup
Refocusing magnet
Beam
Energy defining slits
Collimator
10 ft
Target
Faraday cup
45°
Electron beam
Mica strip
Radius
28.40 mm or
63.5 mm
XBL6810-6875

Fig. 1

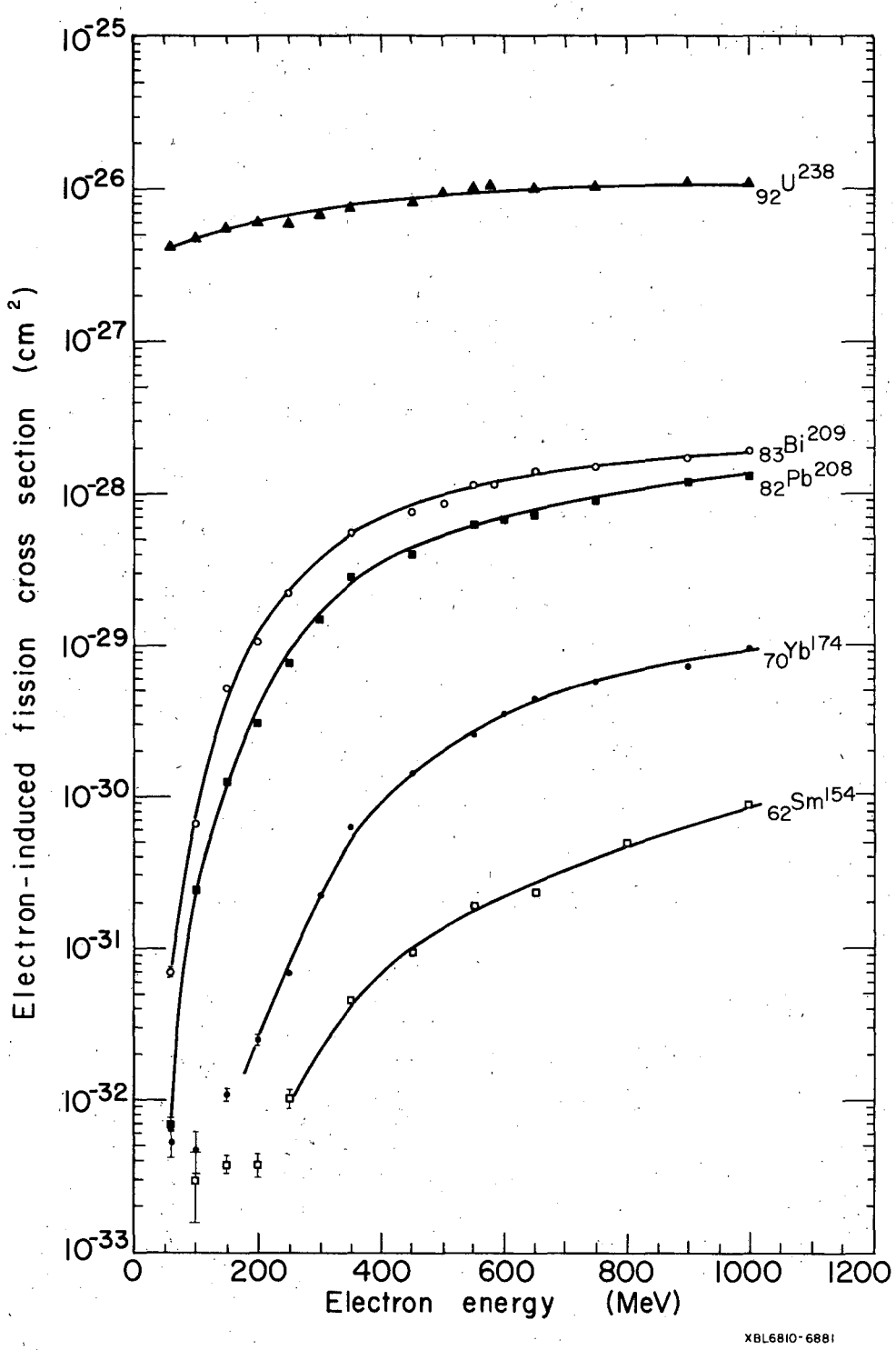
Electron-induced fission cross section (cm²)
10⁻²⁵
10⁻²⁶
10⁻²⁷
10⁻²⁸
10⁻²⁹
10⁻³⁰
10⁻³¹
10⁻³²
10⁻³³
0
200
400
600
800
1000
1200
Electron energy (MeV)
92U238
83Bi209
82Pb208
70Yb174
62Sm154
XBL6810-6881

Fig. 2

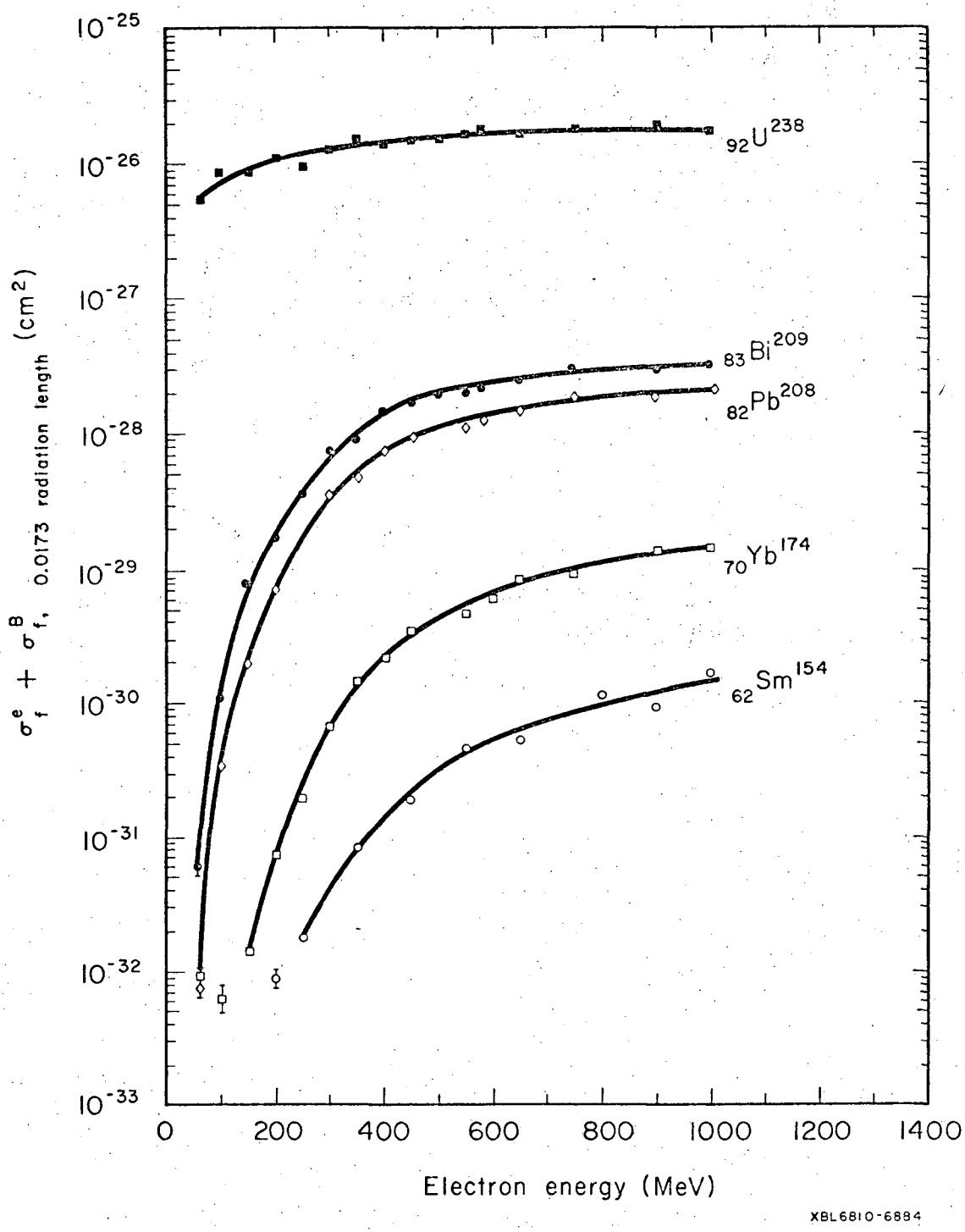
10^{-25}
10^{-26}
10^{-27}
10^{-28}
10^{-29}
10^{-30}
10^{-31}
10^{-32}
10^{-33}
$\sigma_f^e + \sigma_f^B$, 0.0173 radiation length (cm^2)
$_{92}U^{238}$
$_{83}Bi^{209}$
$_{82}Pb^{208}$
$_{70}Yb^{174}$
$_{62}Sm^{154}$
0
200
400
600
800
1000
1200
1400
Electron energy (MeV)
XBL6810-6884

Fig. 3

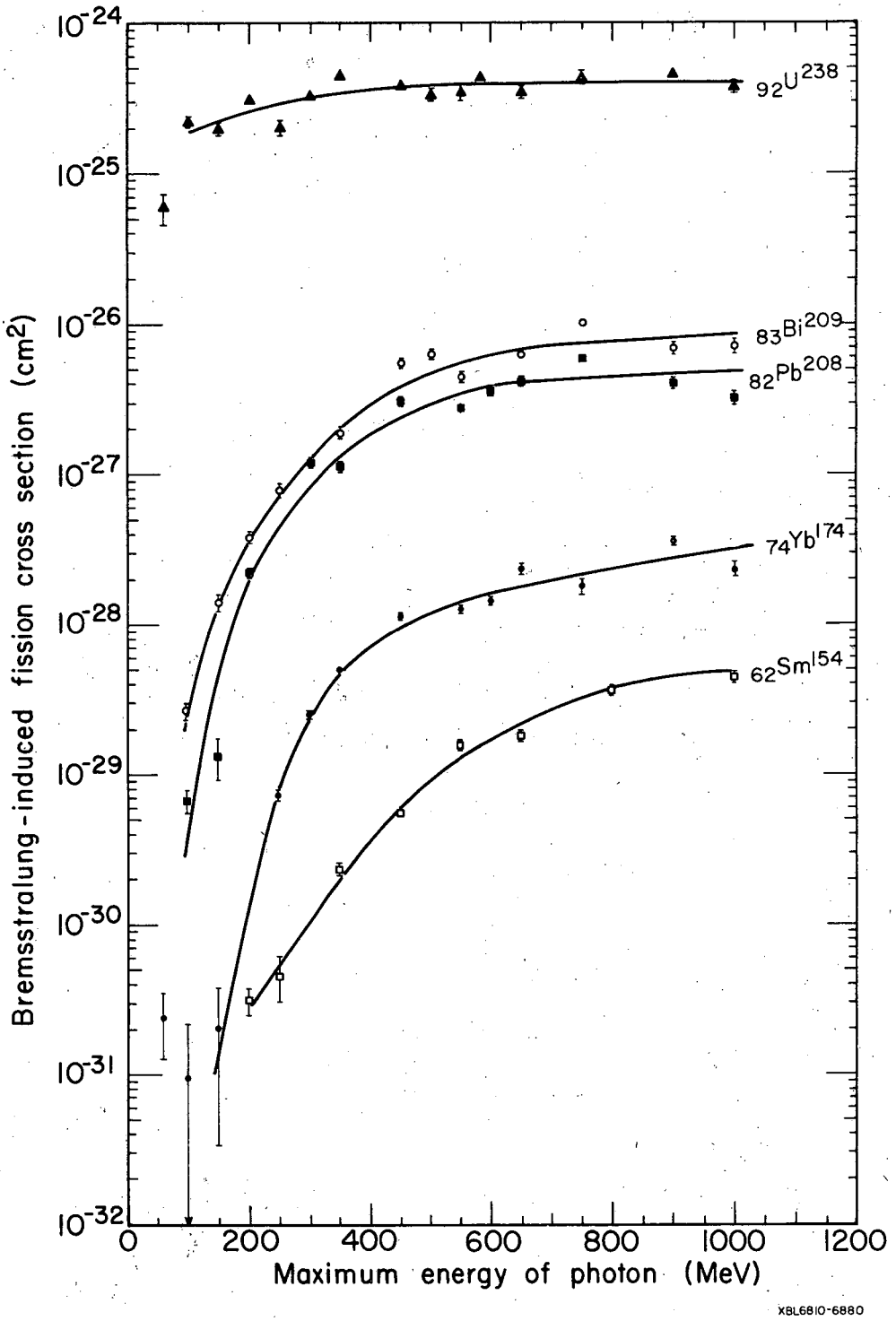
Bremsstralung-induced fission cross section (cm²)
10⁻²⁴
10⁻²⁵
10⁻²⁶
10⁻²⁷
10⁻²⁸
10⁻²⁹
10⁻³⁰
10⁻³¹
10⁻³²
0
200
400
600
800
1000
1200
Maximum energy of photon (MeV)
92U238
83Bi209
82Pb208
74Yb174
62Sm154
XBL6810-6880

Fig. 4

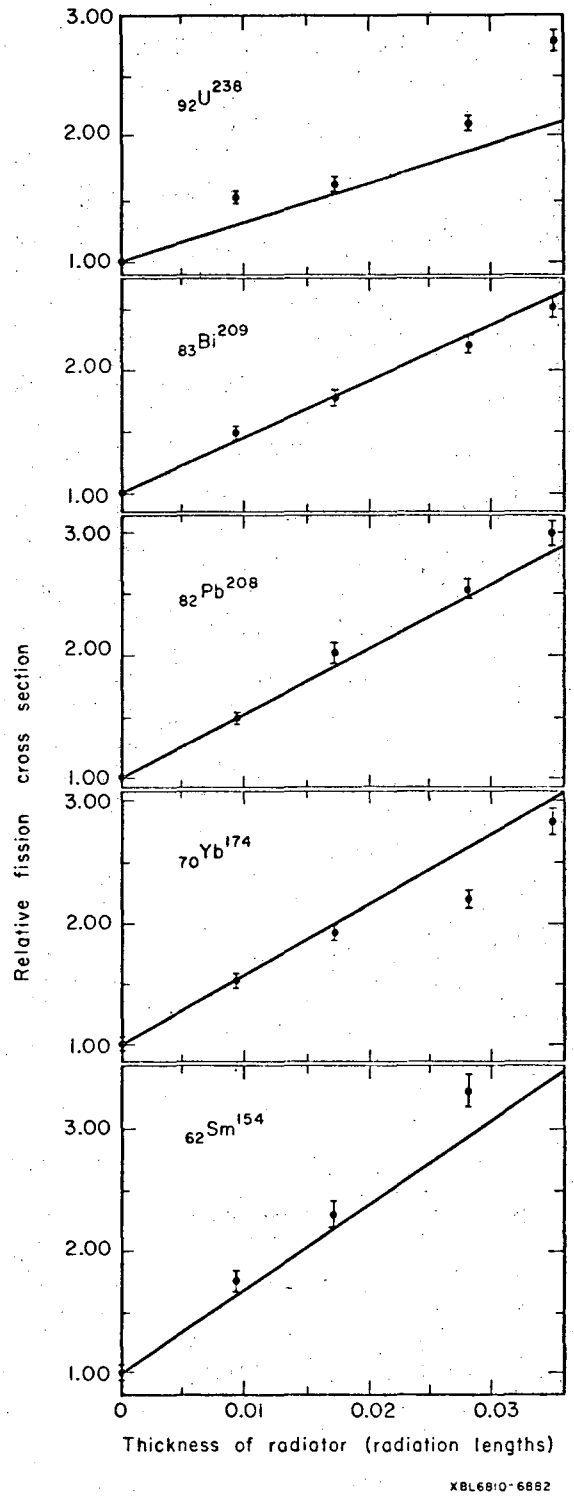
3.00
2.00
1.00
$_{92}U^{238}$
$_{83}Bi^{209}$
$_{82}Pb^{208}$
$_{70}Yb^{174}$
$_{62}Sm^{154}$
Relative fission cross section
0
0.01
0.02
0.03
Thickness of radiator (radiation lengths)
XBL6810-6882

Fig. 5

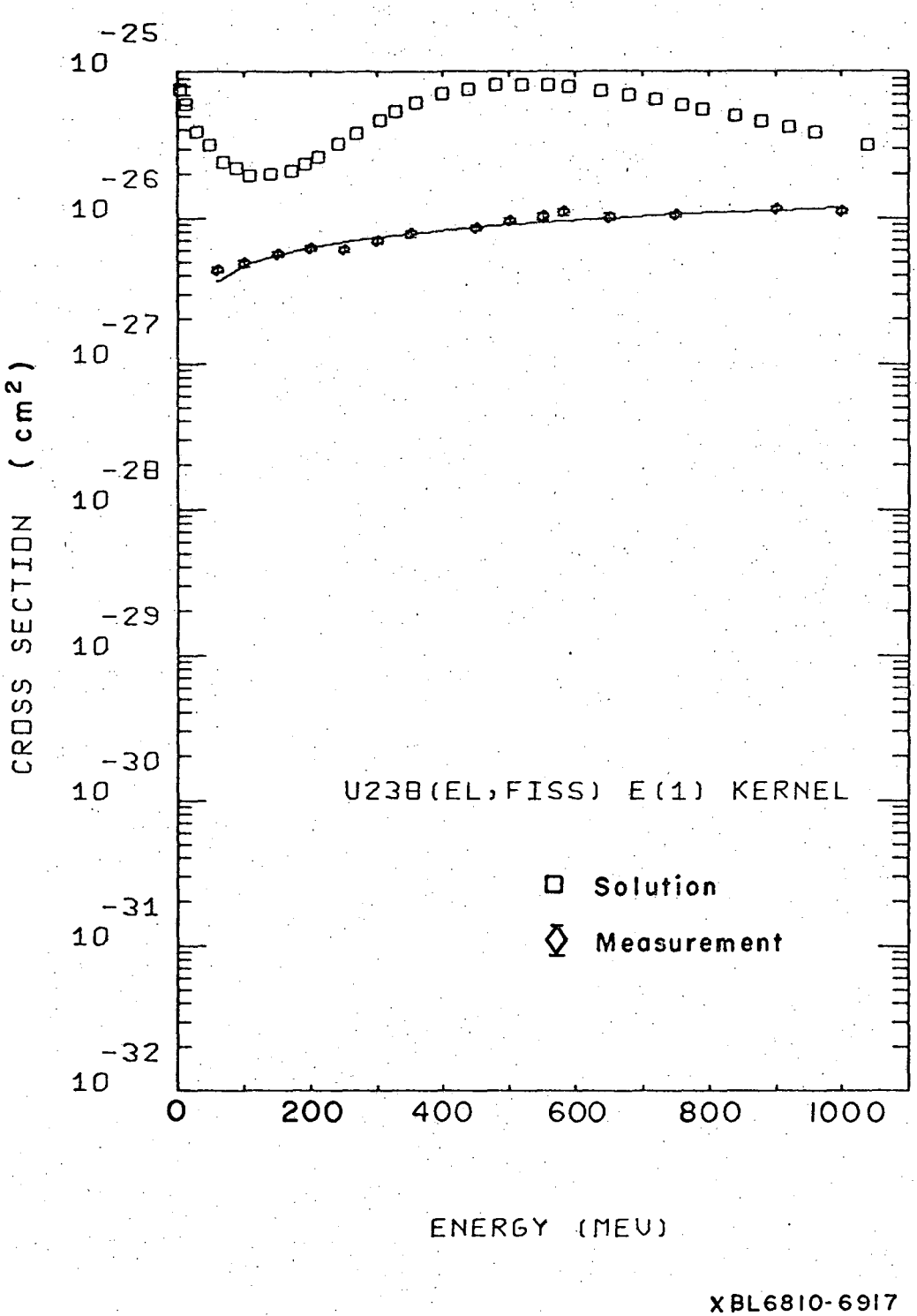

XBL6810-6917

Fig. 6

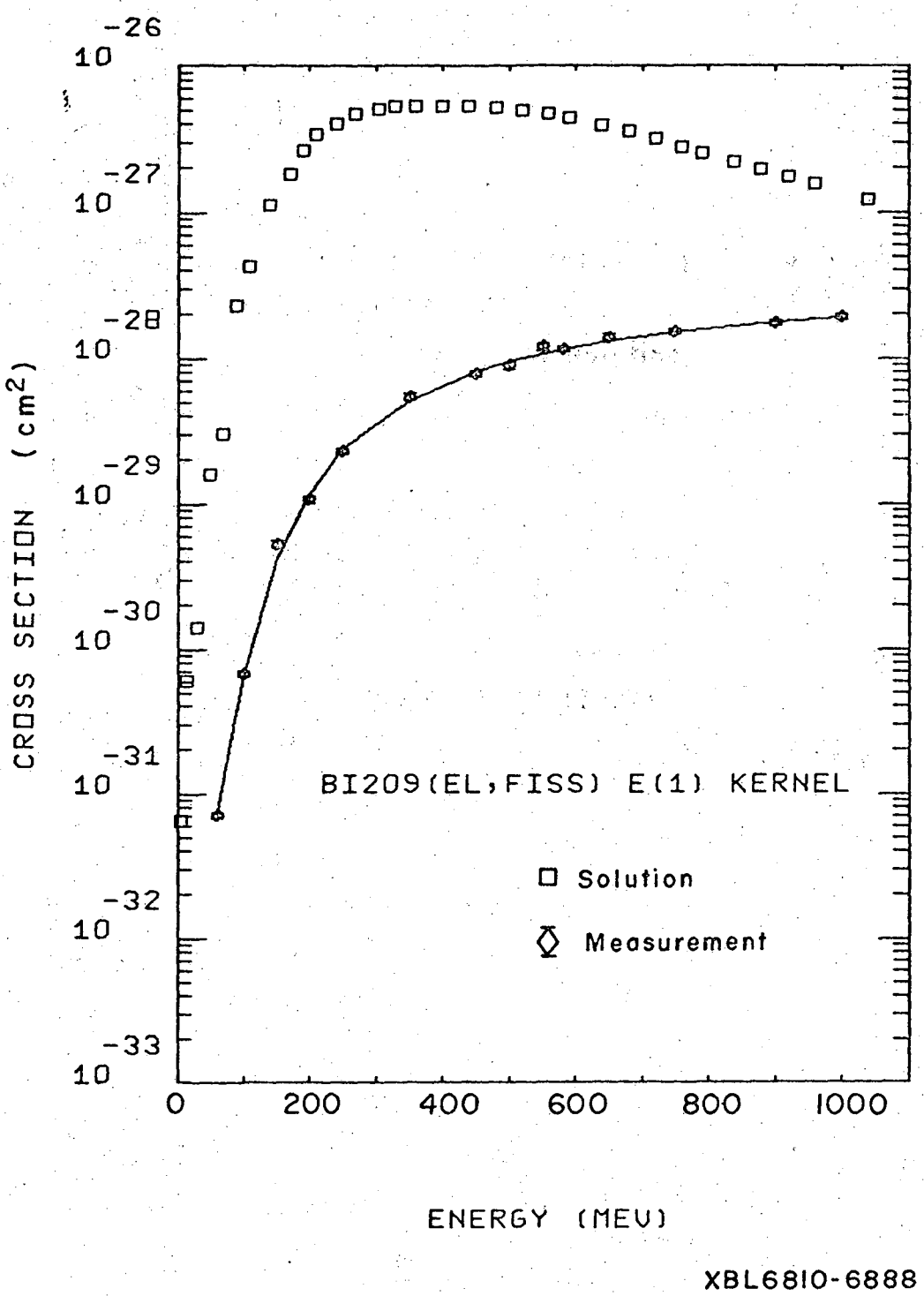

XBL6810-6888

Fig. 7

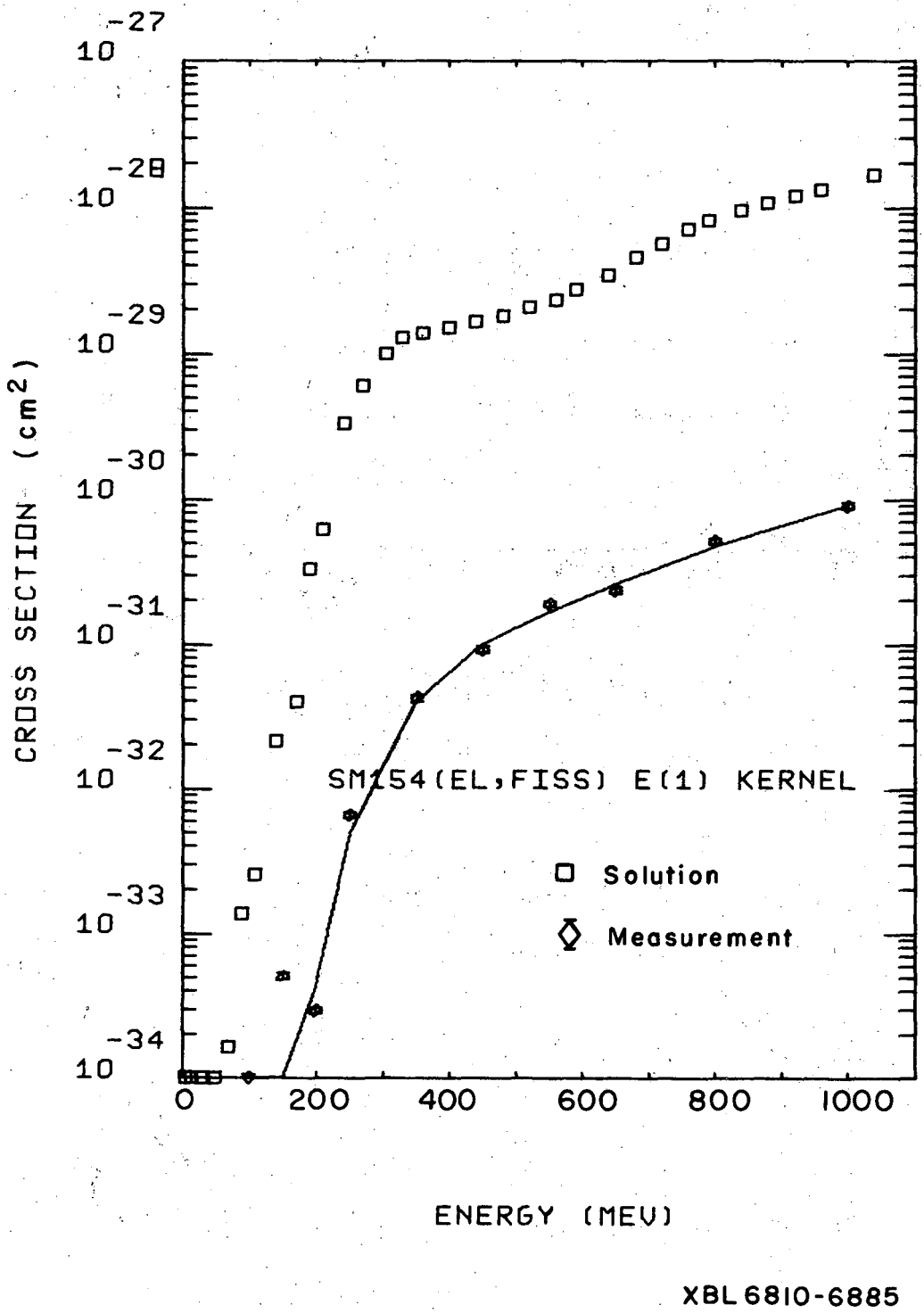

XBL 6810-6885

Fig. 10

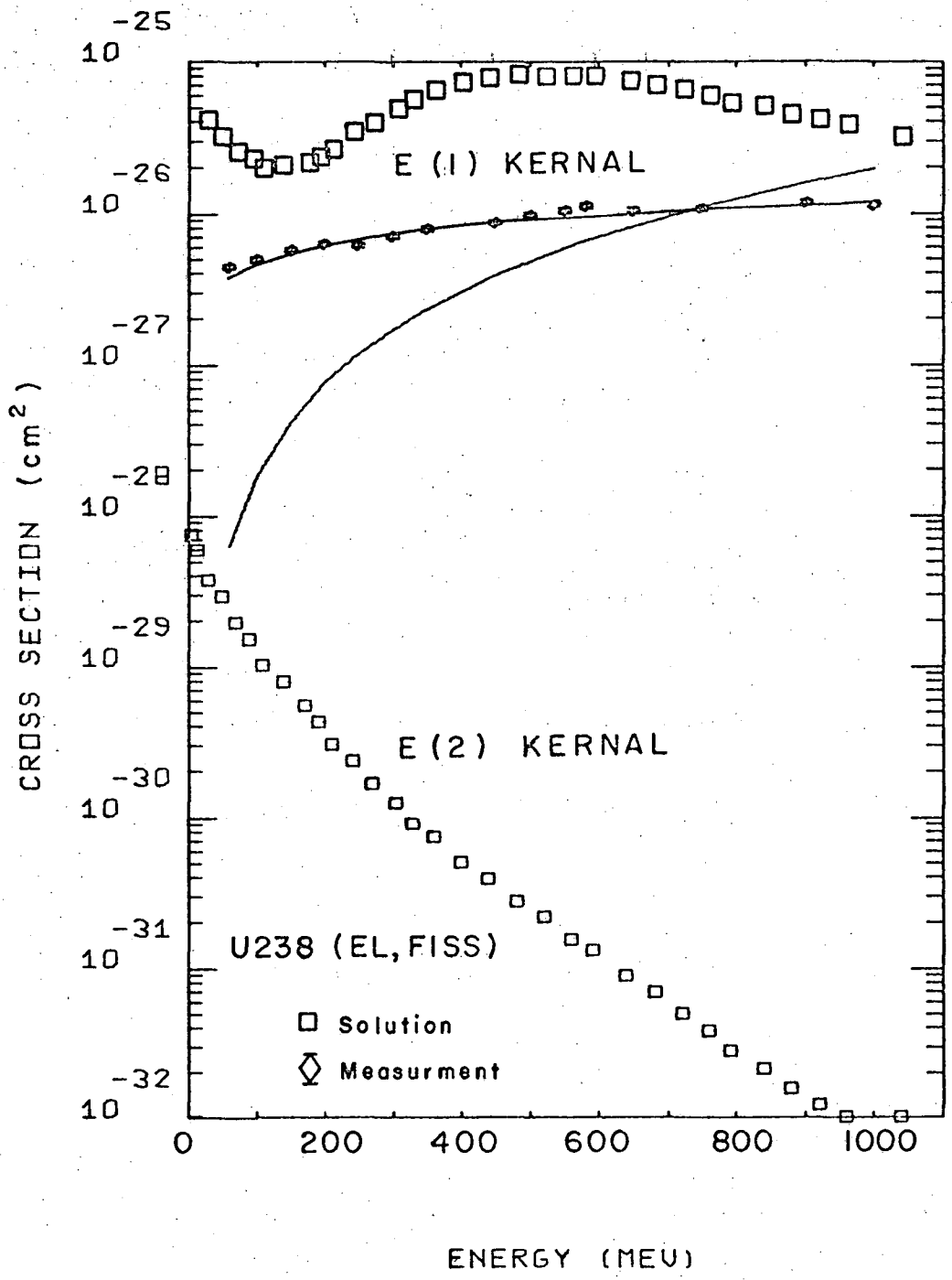

XBL6810-6919

Fig. 11

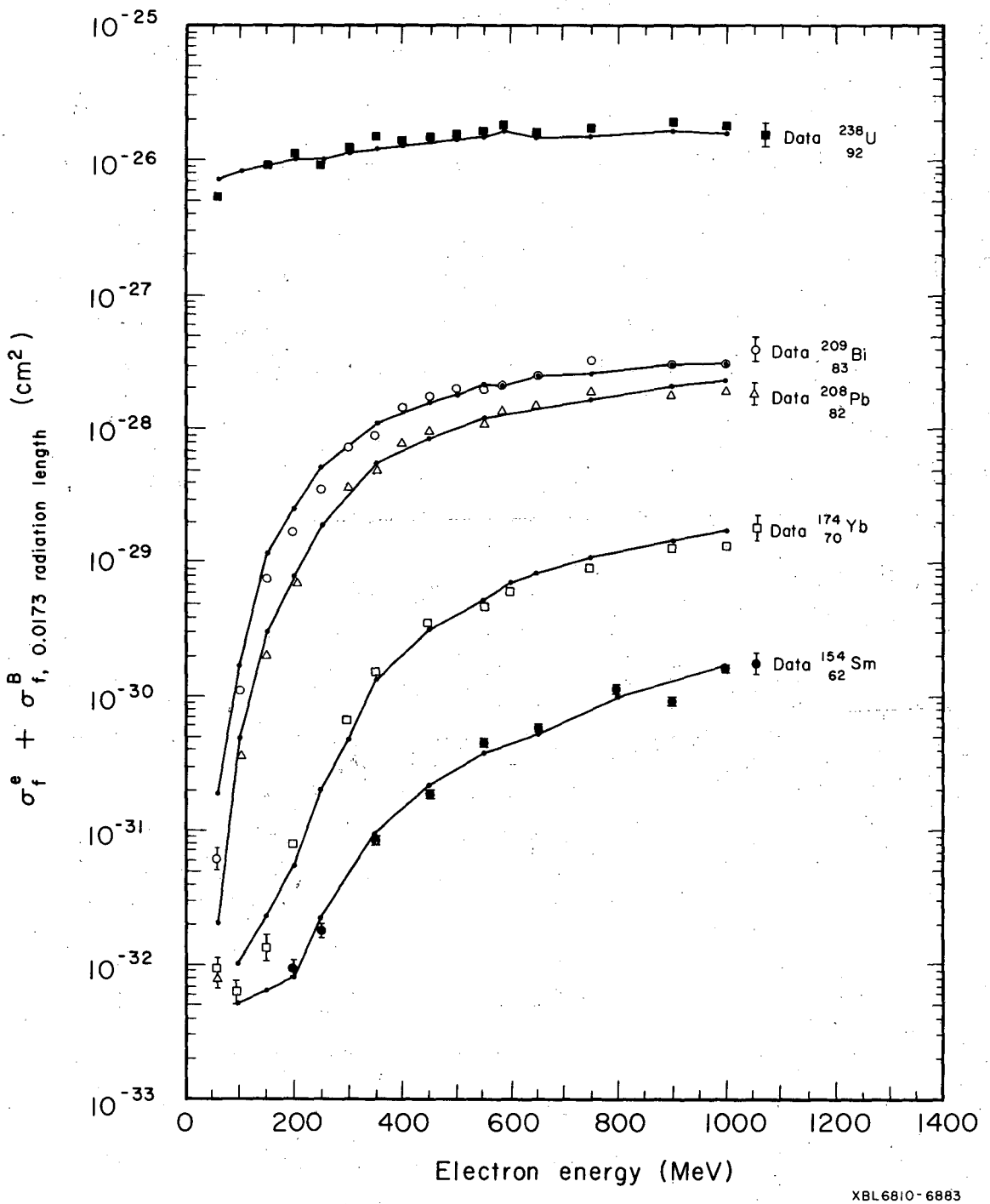
10^{-25}
10^{-26}
10^{-27}
10^{-28}
10^{-29}
10^{-30}
10^{-31}
10^{-32}
10^{-33}
$\sigma_f^e + \sigma_{f,\ 0.0173\ \text{radiation length}}^B$ (cm^2)
0
200
400
600
800
1000
1200
1400
Electron energy (MeV)
Data $^{238}_{92}$U
Data $^{209}_{83}$Bi
Data $^{208}_{82}$Pb
Data $^{174}_{70}$Yb
Data $^{154}_{62}$Sm
XBL6810-6883

Fig. 12

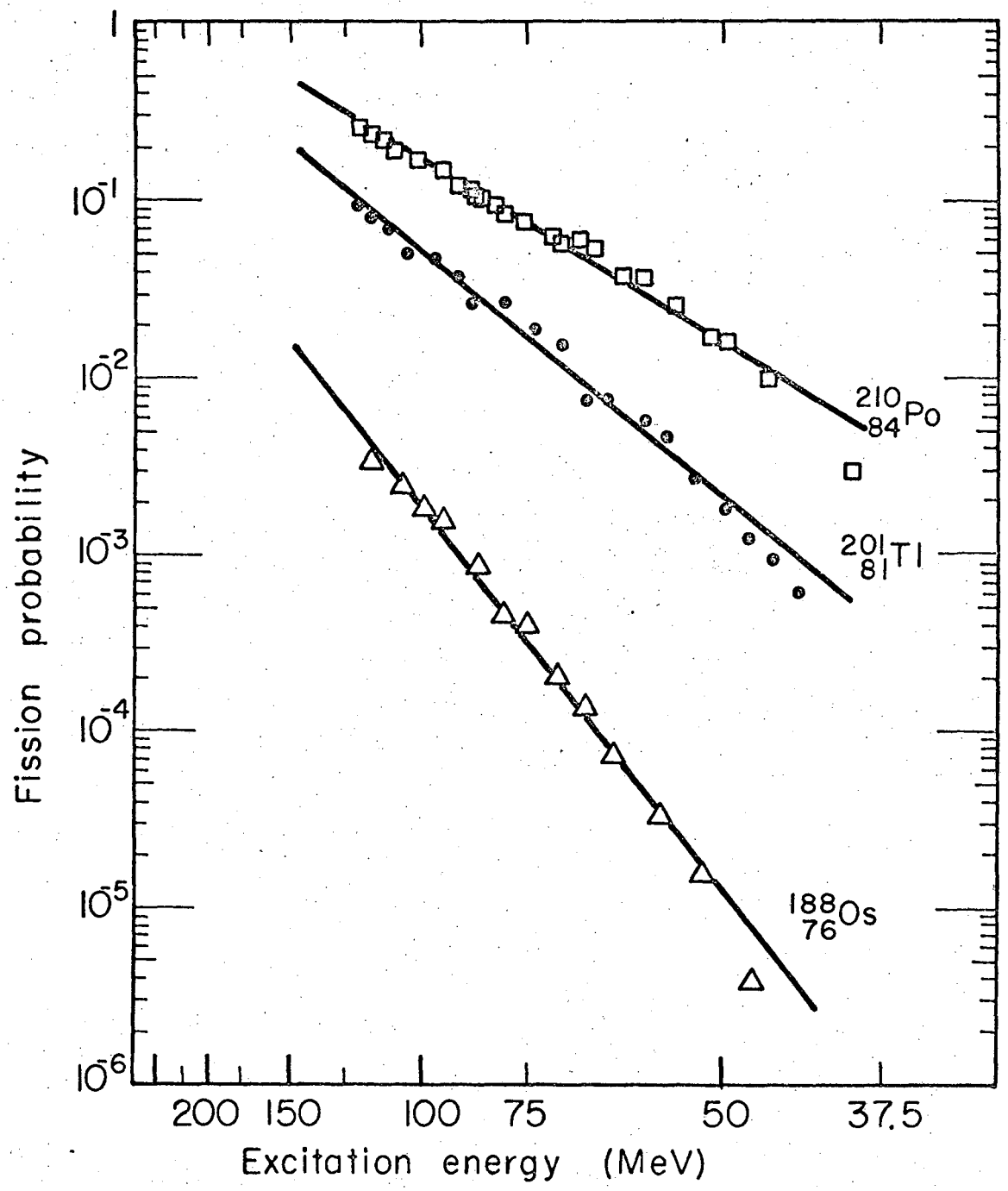

XBL 6810-6879

Fig. 13

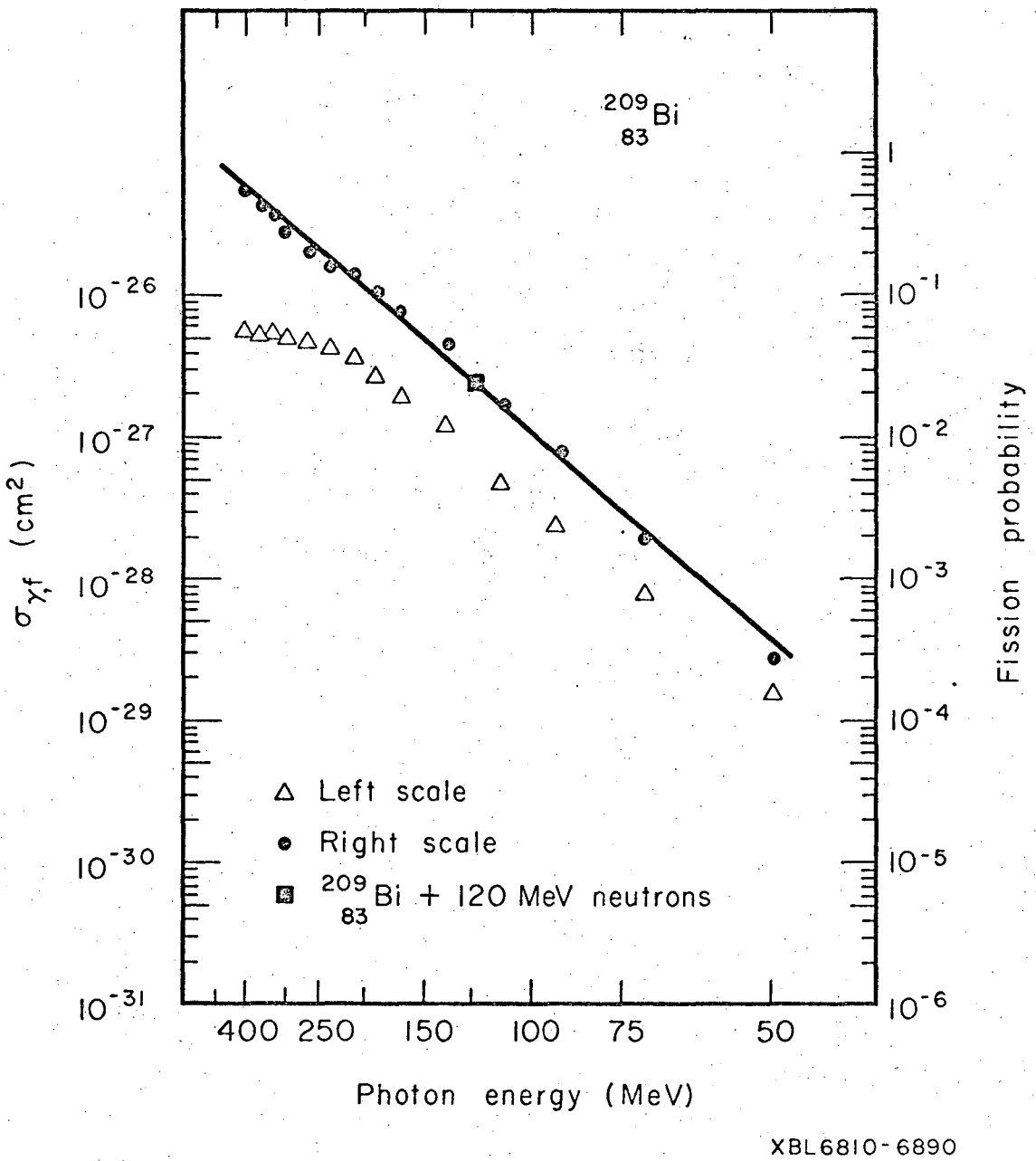
$^{209}_{83}$Bi
10^{-26}
10^{-27}
10^{-28}
10^{-29}
10^{-30}
10^{-31}
$\sigma_{\gamma,f}$ (cm^2)
1
10^{-1}
10^{-2}
10^{-3}
10^{-4}
10^{-5}
10^{-6}
Fission probability
400 250 150 100 75 50
Photon energy (MeV)
Left scale
Right scale
$^{209}_{83}$Bi + 120 MeV neutrons
XBL6810-6890

Fig. 14

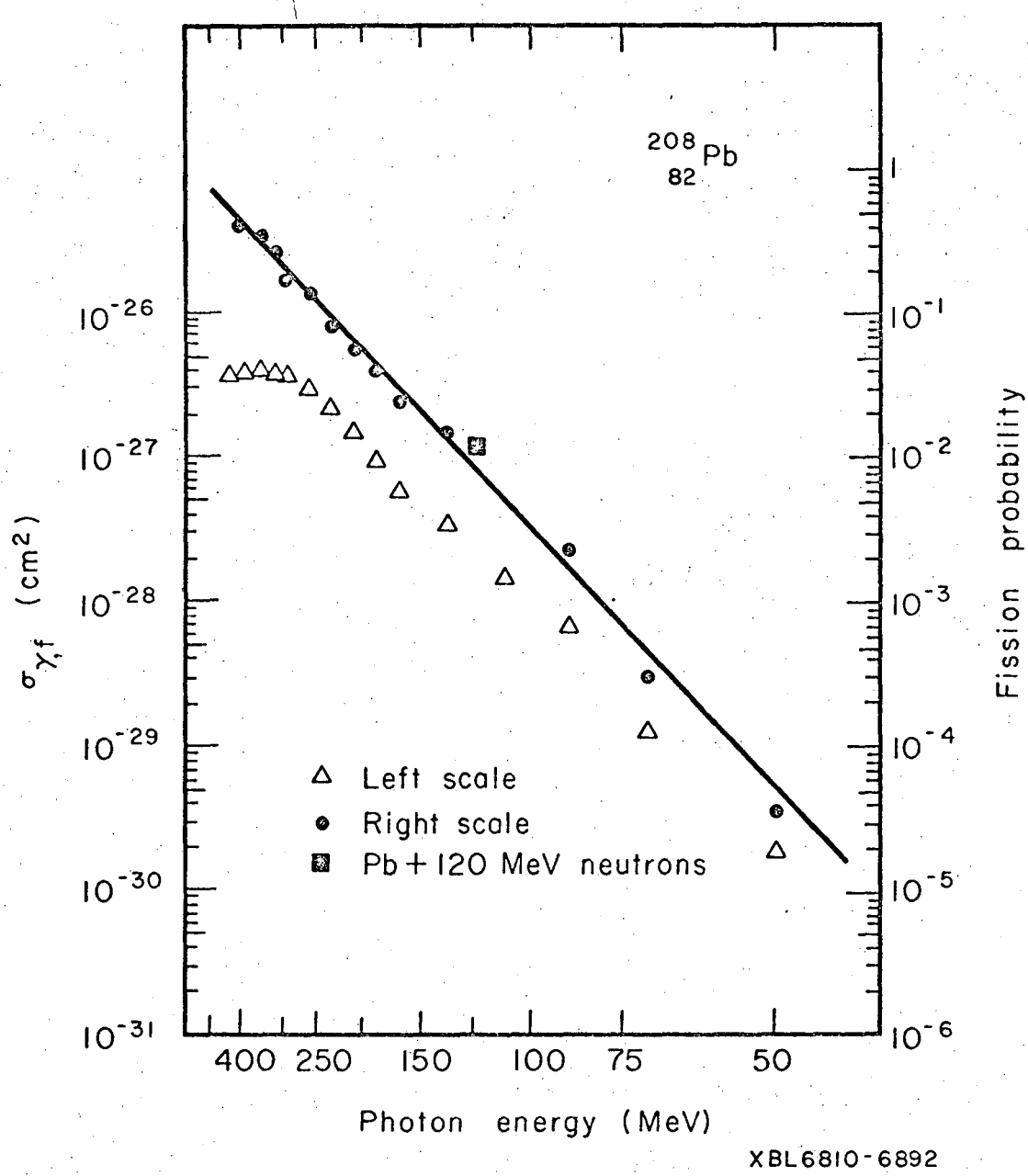
$^{208}_{82}$Pb
10^{-26}
10^{-27}
10^{-28}
10^{-29}
10^{-30}
10^{-31}
$\sigma_{\gamma,f}$ (cm^2)
1
10^{-1}
10^{-2}
10^{-3}
10^{-4}
10^{-5}
10^{-6}
Fission probability
Left scale
Right scale
Pb + 120 MeV neutrons
400 250 150 100 75 50
Photon energy (MeV)
XBL6810-6892

Fig. 15

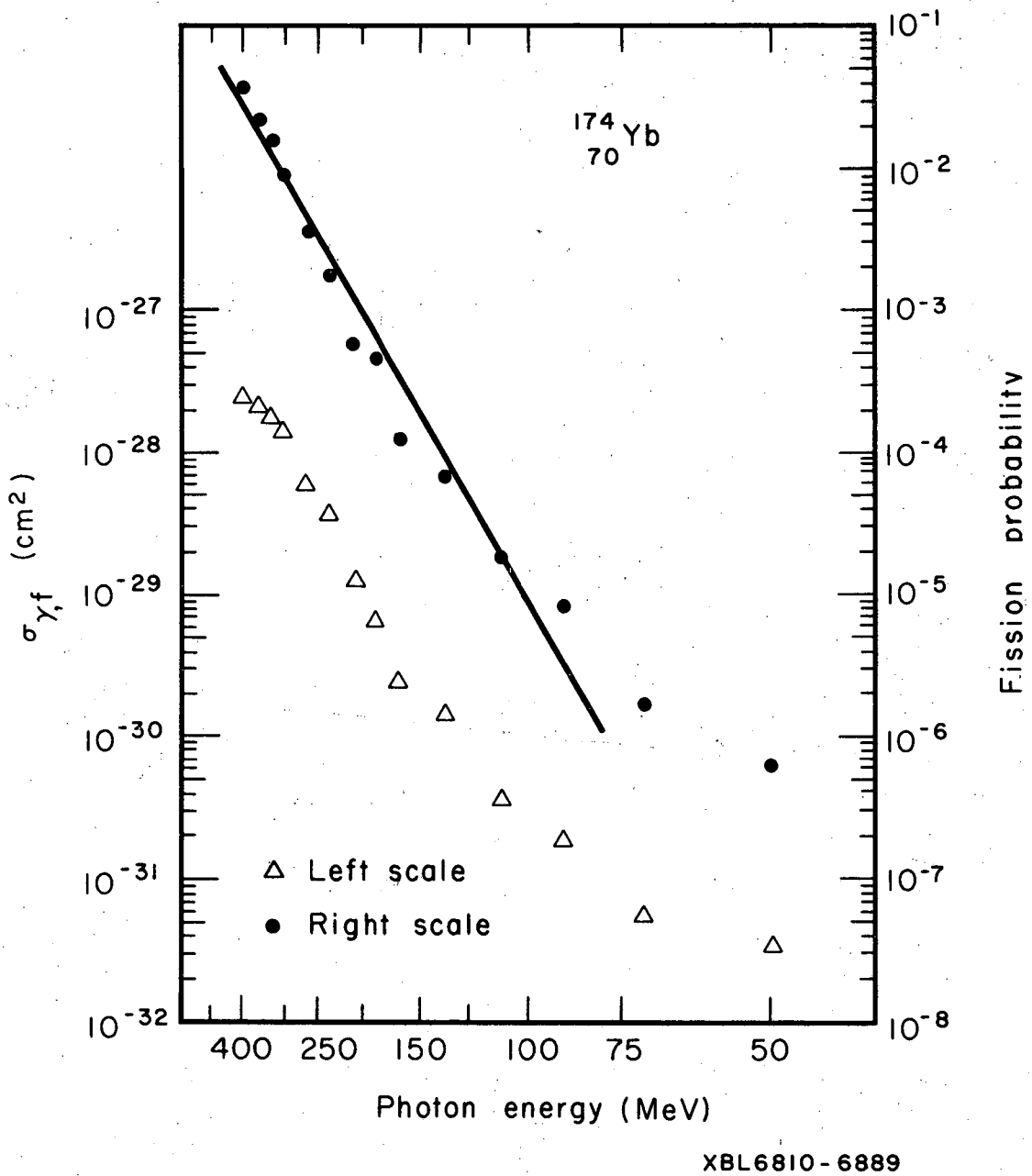
$^{174}_{70}$Yb
10^{-27}
10^{-28}
10^{-29}
10^{-30}
10^{-31}
10^{-32}
$\sigma_{\gamma,f}$ (cm^2)
10^{-1}
10^{-2}
10^{-3}
10^{-4}
10^{-5}
10^{-6}
10^{-7}
10^{-8}
Fission probability
Left scale
Right scale
400 250 150 100 75 50
Photon energy (MeV)
XBL6810-6889

Fig. 16

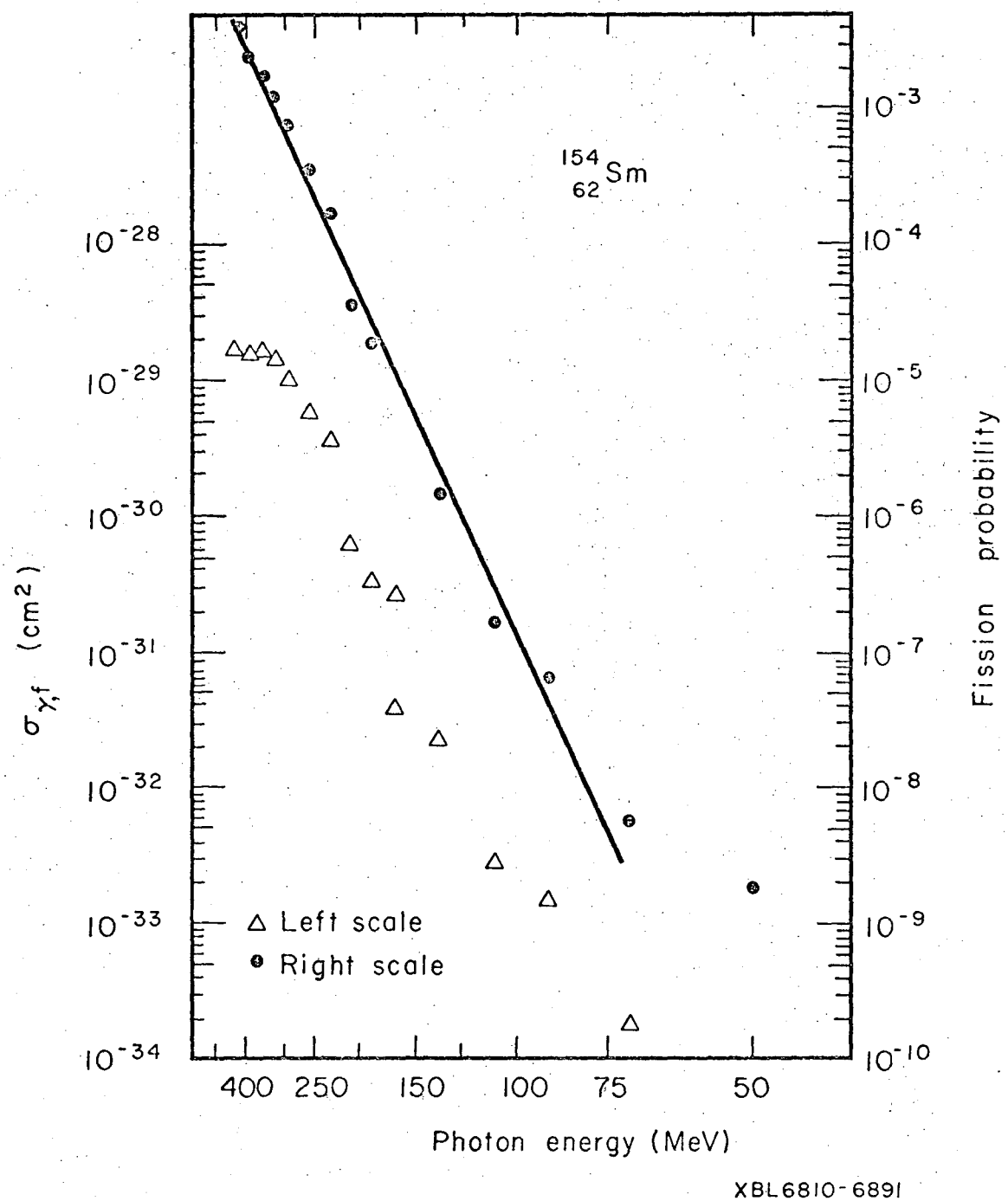
$^{154}_{62}$Sm
10^{-28}
10^{-29}
10^{-30}
10^{-31}
10^{-32}
10^{-33}
10^{-34}
$\sigma_{\gamma,f}$ (cm^2)
10^{-3}
10^{-4}
10^{-5}
10^{-6}
10^{-7}
10^{-8}
10^{-9}
10^{-10}
Fission probability
△ Left scale
● Right scale
400 250 150 100 75 50
Photon energy (MeV)
XBL6810-6891

Fig. 17

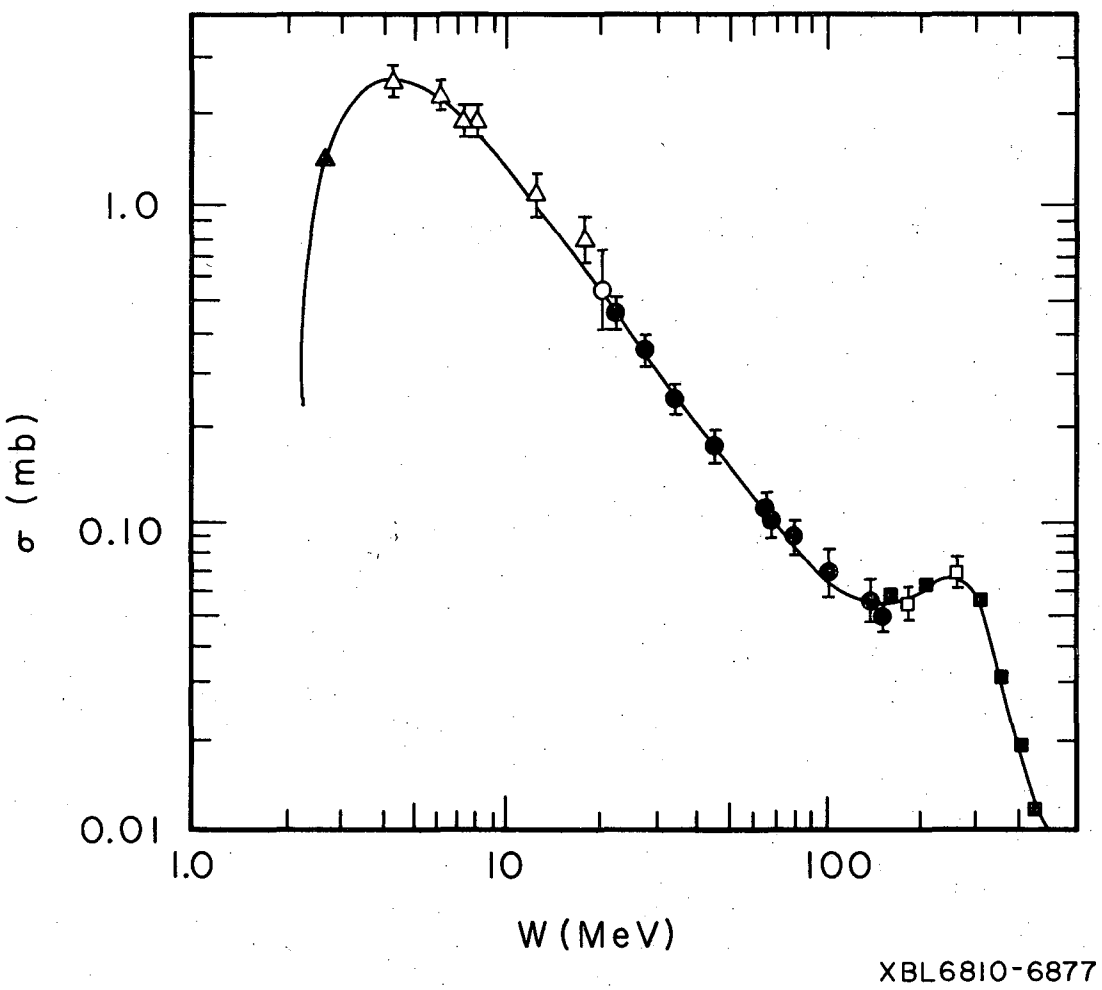

Fig. 18

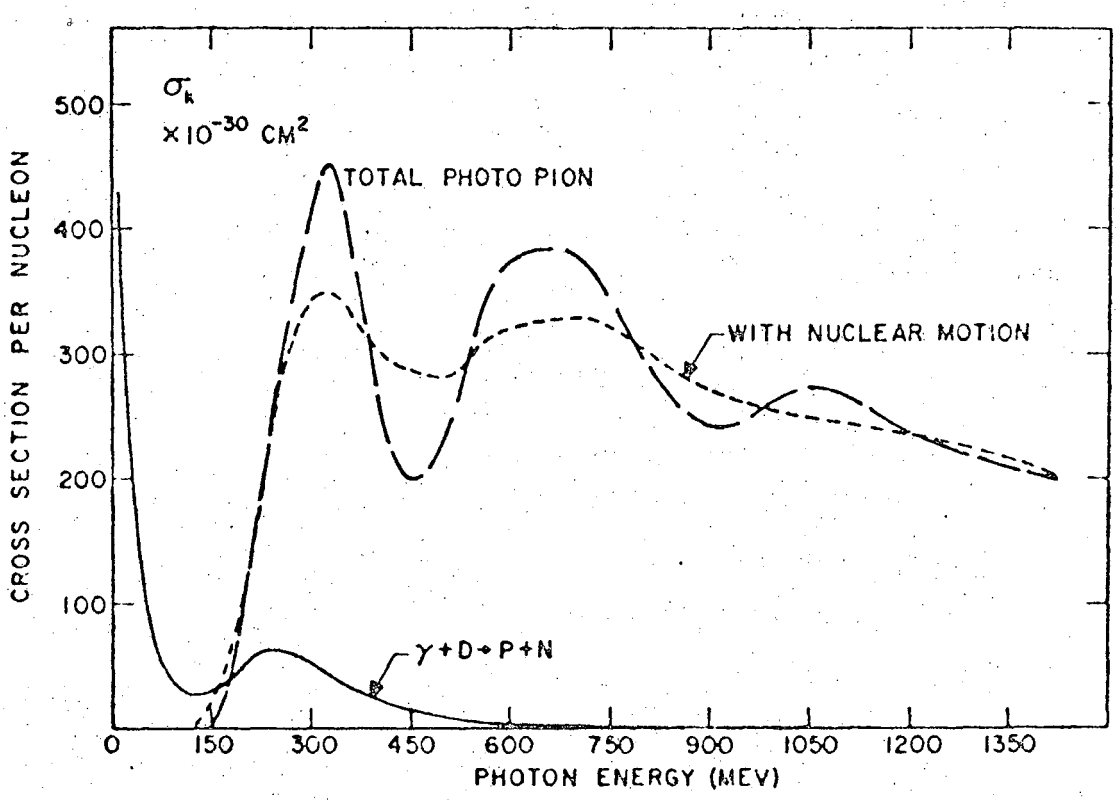

XBL6810-6876

Fig. 19